Motional Narrowing of Electron Spin Resonance in Single-Walled Carbon Nanotubes

W. D. Rice,[1,2] R. T. Weber,[3] S. Nanot,[1,2] P. Nikolaev,[4] S. Arepalli,[4] A.-L. Tsai,[5] and J. Kono[1,2,*]
[1] *Department of Electrical and Computer Engineering, Rice University, Houston, Texas 77005, USA*
[2] *Department of Physics and Astronomy, Rice University, Houston, Texas 77005, USA*
[3] *Bruker BioSpin Corporation, Billerica, Massachusetts, 01821 USA*
[4] *Department of Energy Science, Sungkyunkwan University, Suwon 440-746, South Korea*
[5] *University of Texas Medical School, Houston, Texas 77005, USA*
(Dated: January 25, 2013)

arXiv:1105.5095v2 [cond-mat.mes-hall] 20 Dec 2011

We have measured electron spin resonance in bulk single-walled carbon nanotubes. The linewidth was observed to narrow by as much as ∼50%, as the temperature was increased from 3 to 300 K. From the linewidth change versus temperature, we find the hopping frequency to be 285 GHz. Although the spins are mobile, they are still a finite-level-spin species, as indicated by the Curie law temperature dependence of the spin susceptibility. We show that the Dysonian lineshape asymmetry follows a three-dimensional variable-range hopping behavior from 3 to 20 K and extract a localization length of the hopping spins to be ∼100 nm.

PACS numbers: 76.30.-v, 72.20.Ee, 73.63.Fg

Understanding spin dynamics is key to a broad range of modern problems in condensed matter physics [1–6] and applied sciences [7, 8]. Spin transport is a sensitive probe of many-body correlations as well as an indispensable process in spintronic devices. Confined spins, particularly those in one dimension (1D), are predicted to show strong correlations [2, 4–6, 9] and long coherence times [3]. Single-walled carbon nanotubes (SWCNTs) are ideal materials for studying 1D spin physics due to their long mean free paths and weak spin-orbit coupling [10]. Exotic spin properties in metallic SWCNTs at low temperatures and high magnetic fields have been predicted, including the appearance of a peak splitting in the spin energy density spectrum, which can be used to probe spin-charge separation in Luttinger-liquid theory [4–6].

One method for studying spin dynamics is electron spin resonance (ESR), which provides information on spin-orbit coupling, phase relaxation time, spin susceptibility, and spin diffusion. Many theoretical and experimental ESR studies of SWCNTs have been performed over the past decade [5, 6, 11–17]. Unfortunately, experimental ESR studies of SWCNTs have been difficult due to sample issues, such as the presence of trace amounts of ferromagnetic catalyst particles and SWCNT sample inhomogeneity. Substantial conflicts have thus emerged in the literature, such as the temperature (T) dependence of the spin susceptibility and ESR lineshape [11–17].

Here, we show that the probed spins in SWCNTs are localized species that undergo phonon-assisted hopping. Specifically, we find that the ESR linewidth becomes smaller as T is increased, a hallmark of the phenomenon of motional narrowing [18, 19]. This spin mobility accounts for the Dysonian lineshape [20] seen throughout the full T range examined. In addition, we observe that the spin susceptibility displays a Curie law ($\propto 1/T$) behavior, suggesting that, while spins may move about the sample, they are still a finite-level system. The Dysonian lineshape asymmetry parameter, which is proportional to the conductance of the probed spins, is shown to follow the 3D variable-range hopping (VRH) trend. From our data, we find the density of states at the Fermi energy to be $\sim 10^{19}$ states/eV-cm^3, and we estimate the localization length of the spins to be $\sim$ 100 nm.

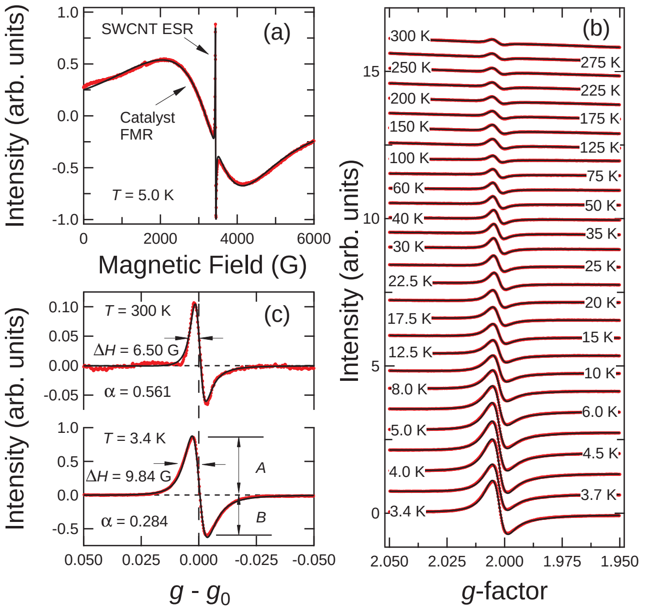

FIG. 1: (color online) ESR scans of SWCNT powder sample. (a) A raw spectrum at 5.0 K across a 6000 G applied field range shows a sharp ESR peak on top of a large FMR background. (b) Raw detailed scans with Dysonian lineshape fits for all temperatures investigated. Each trace is intentionally offset for clarity. (c) Comparison of highest and lowest temperature lineforms. The linewidth, A, B, and α (see text for definitions) are given for both traces for comparison.

Data was taken using a Bruker EMX spectrometer using a cavity in the TE$_{102}$ mode in the X-band (9.6 GHz) regime. For temperatures below 125 K, we used 200 μW of microwave power, while for temperatures 125 K and above, we used 1 mW. In all cases, we were in the linear absorption regime as shown by microwave power dependent scans performed on the sample across the full temperature range. Our sample consisted of acid purified laser oven SWCNTs in powder form [21]. We compacted the powder by ultracentrifugation after immersing the SWCNTs in water. This procedure immobilized the nanotubes into a condensed pellet without the need for direct mechanical compaction. In addition, adsorbed gases and water were removed by annealing the sample for 24 hours at 115°C under vacuum with a small argon gas flow. To protect the sample from contact with the outside environment, the 630 μg (0.24 g/cm^3) SWCNT sample ($\sim$27% of which is SWCNTs [21], equivalent to 170 μg or 0.064 g/cm^3) was submerged in mineral oil under helium gas in a sealed quartz tube [22].

ESR spectra (Fig. 1) were taken at discrete temperatures from 3.4 to 300 K. We used 2,2-diphenyl-1-picrylhydrazyl (DPPH) as a frequency standard to calibrate the applied magnetic field, H_0, and a 1 mM $CuSO_4{\cdot}5H_2O$ standard as a concentration standard to extract the spin susceptibility. As seen in Fig. 1(a), a broad ferromagnetic resonance (FMR) dominates the spectrum. The FMR is tentatively assigned to the nickel and cobalt catalyst particles remaining in the acid-purified sample. By closely scanning H_0 around the SWCNT ESR peak, a detailed study of the SWCNT ESR lineshape can be performed as a function of T, as seen in Fig. 1(b). Both the linewidth and peak-to-peak amplitude become larger as T is decreased, while the line-center position (g-factor, or simply, g) shows little T dependence, staying close to the free-electron g-factor of 2.0023 for each different temperature examined. The ESR line is asymmetric, as seen in Fig. 1(c), having what is often referred to as a Dysonian lineshape [20] indicating movement of the electrons in and out of the H_1 perturbing magnetic field.

To gain further quantitative understanding, we numerically fit each ESR scan. The slowly varying FMR background was fit by a combination of two large-linewidth ($\sim$ 1000 G) Lorentzians. The SWCNT ESR feature was fit using the weak form of the Dysonian lineshape [16, 23]:

$$\frac{d\chi}{dH_0} = \left(\frac{\cos\varphi}{\Delta H^2}\right)\frac{-2y + (1-y^2)\tan\varphi}{(1+y^2)^2}, \tag{1}$$

where $y = \frac{H_0 - H_r}{\Delta H}$, H_r is the resonance field, ΔH is the half-width and is equal to $\frac{1}{\gamma T_2}$, with $\gamma = \frac{g\mu_B}{\hbar}$ and μ_B the Bohr magneton. The weak form of Dysonian can be used here, because the conductivity and diffusion of the electrons in the SWCNT powder are both low as compared to a traditional metal. Nevertheless, unlike traditional magnetic resonance where the signal depends entirely on the imaginary part of the ac spin susceptibility, χ'', the Dysonian lineshape is also influenced by the real component, χ'. Taking the ac susceptibility, χ, to be

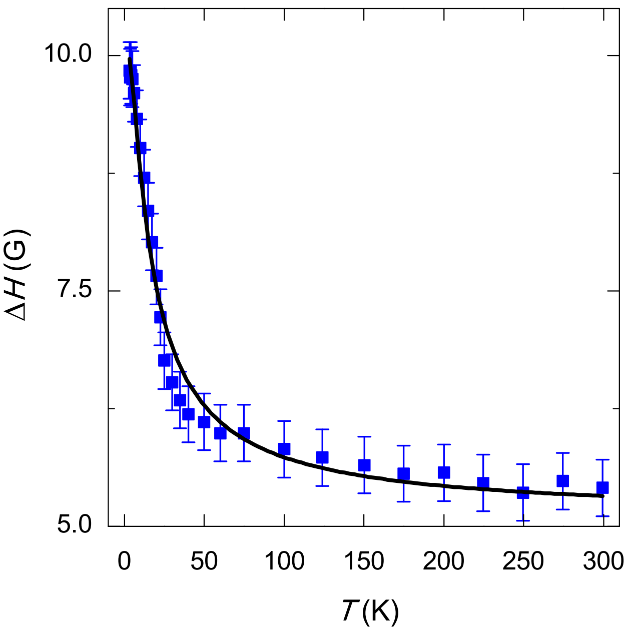

FIG. 2: (Color online) ESR linewidth as a function of temperature (T). The steep rise in ΔH as T is decreased shows that the spin dephasing time becomes shorter as the lattice energy is decreased. A theoretical fit based on variable range hopping, given by the black line, well-describes the data.

$$\chi = \chi''\cos\varphi + \chi'\sin\varphi, \tag{2}$$

we define $\alpha \equiv \tan\varphi$, which is a dimensionless measure of the relative contribution of the real part (= 0 for traditional ESR). This parameter is also a measure of the asymmetry of the lineshape, and $A/B \approx 1 + \alpha$ when $\alpha \ll 1$, where A and B are defined in Fig. 1(c). Furthermore, it can be related to the electrical conductivity of the probed spins, σ_{spin}, as $\alpha \propto \sigma_{\text{spin}}$, allowing us to compare transport and spin resonance results [23].

From the numerical fitting, we extract ΔH, α, and the mass spin susceptibility, χ_g. Unlike previous studies of ESR in nanotubes, ΔH changes substantially with T. As Fig. 2 shows, as T is increased, ΔH rapidly decreases until $\sim$25 K, whereupon the linewidth begins to decrease more slowly up to 300 K. This decrease of the ESR linewidth with increasing T is consistent with the phenomenon of motional narrowing [18, 19], which occurs because the dephasing time of the spins can change as their translational energy is altered. At high T, the spins move rapidly, allowing for less time around dephasing centers, thus reducing the interaction between the probed spins and the dephasing centers. This decreased interaction gives a longer spin dephasing time (T_2), which in turn narrows the lineshape. Conversely, at low T, the spins are moving more slowly, which broadens the line.

To understand the observation of motional narrowing more quantitatively, we start with a generalized narrowing model [24, 25]:

$$\Delta H \simeq \frac{\Delta H_p^2}{\Delta H_e}, \tag{3}$$

where ΔH_p is the amplitude of the perturbations and ΔH_e describes the rate of spin motion. Equation (3) was originally derived to describe exchange narrowing or motional narrowing from spin diffusion. However, spin diffusion can be described in terms of phonon-activated, variable range hopping with a probability, p_{VRH}, that is proportional to $\exp\left(-2R/\xi - \Delta E/k_{\mathrm{B}}T\right)$ [26–28]. Here, R is the hopping distance, ξ is the localization length, ΔE is the average spacing between energy levels, and k_{B} is the Boltzmann constant. Combining this hopping conduction with Eq. (3) and adding an offset, ΔH_0, gives [29, 30]

$$\Delta H = \Delta H_0 + \frac{A}{\Delta E \times \left[1 + \coth\left(\frac{\Delta E}{2k_{\mathrm{B}}T}\right)\right]} \tag{4}$$

where ΔH_0 is the high-T ("metallic") asymptotic limit of the linewidth and A is independent of T. As Fig. 2 shows, Eq. (4) fits very well to the observed linewidth. We find A to be 11.6±0.8 meV-G and $\Delta H_0 = 5.10\pm0.08$ G, with the latter quantity giving a T_2 spin dephasing time of 11.1 ns. The activation energy, ΔE, is 1.18±0.09 meV (13.7 K or 285 GHz). From the value of ΔE, we can get an estimate of how much time (on average) each spin spends at each hopping location, $\tau = \frac{\hbar}{\Delta E} = 558$ fs [31]. If we phenomenologically take $T_2 = n\tau$, where n is the number of jumps before phase coherence is lost, then we can estimate n to be on the order of 10^4 hops, where we have taken T_2 to be ∼10 ns.

The temperature dependence of our linewidth and the fitting to Eq. (4) suggests that we are observing ESR of localized carriers, in a similar fashion to P-doped Si [32, 33] and Ge [29, 30]. In those systems, motional narrowing of ESR is seen at low and intermediate donor concentrations. However, if the impurity concentration is increased, more complicated models would be needed [33, 34]. Additionally, although motional narrowing has not been observed in SWCNTs before, it is reasonable to expect that type of behavior in a system such as nanotubes, since electrons in the basal plane of graphite, in addition to 1D conducting polymers, also show motional narrowing [35–38].

The T dependence of χ_{g} scales with $1/T$, indicating that the spins are a finite-level system (Fig. 3). Indeed, χ_{g} can be fit very well using a Curie law

$$\chi_{\mathrm{g}} = \frac{\mu^2 N}{k_{\mathrm{B}}T}, \tag{5}$$

where μ is the spin magnetic moment and N is the number of probed spins per unit volume. The Curie coefficient, $C = \frac{\mu^2 N}{k_B}$, is found to be $1.11\pm0.01 \times 10^{-7}$ emu-K/g, which agrees with the values from other studies [11, 16]. We do not fit the last two points (at 3.7 and 3.4 K), since it appears as though χ_{g} becomes constant below 4.0 K; further work is needed to establish the low-T spin susceptibility trend. In contradiction with Petit *et al.* [12], we find no evidence of Pauli-like behavior; if we were observing it, we would expect some sort of finite spin susceptibility to remain at high T, as is seen in other 1D systems like protonated polyaniline [39, 40]. The Curie law behavior of the spin susceptibility has been also observed in lightly doped Si and Ge systems [32, 33], as well as intermediately doped Si [41]. At higher doping concentrations, however, deviations from the Curie law are seen, with high doping concentrations displaying Pauli-like trends [34, 41–43].

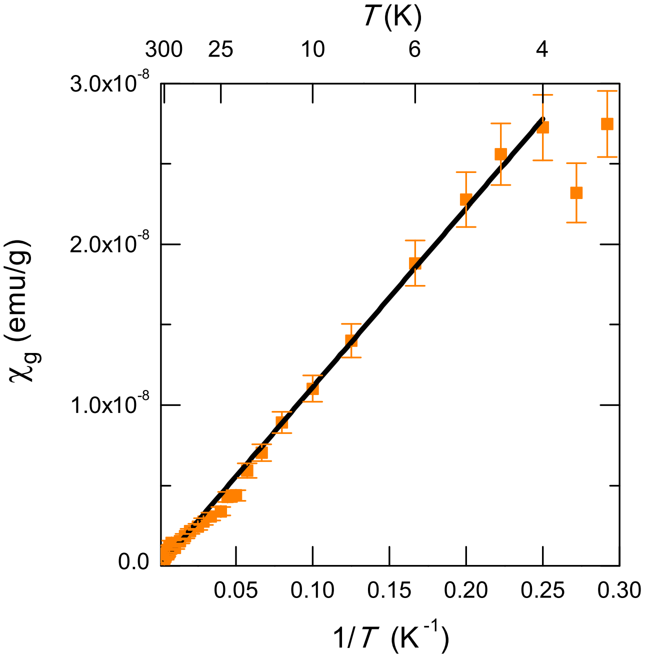

FIG. 3: (Color online) The mass spin susceptibility, χ_{g}, as a function of inverse temperature follows a Curie-law down to 4.0 K, as given by the black best fit line.

Using the spin susceptibility and the measured mass of the sample, we can estimate the number of spins per nanotube. To simplify calculations, we choose to imagine the 170 μg sample made up of entirely (10,10) SWCNTs. Given the Curie constant, we have 3.04×10^{13} probed spins in the sample or 1.14×10^{16} spins/cm^3 since our sample volume is 2.66×10^{-3} cm^3. A given 40 carbon atom unit cell for a (10,10) SWCNT is 0.246 nm in length. If each nanotube is estimated to have a length of 1 μm, we have 0.58 spins per SWCNT, or a Curie coefficient of 3.6×10^{-25} emu-K/SWCNT. This spin density per nanotube suggests that nearly all nanotubes (∼2/3 of the total mass) contribute one spin to the observed signal.

To gain deeper insight into the spin hopping mechanism, we examined the asymmetry Dysonian lineshape parameter, α, which is proportional to the conductance of the probed spins. In particular, we were interested to see if α followed a VRH behavior at low T, which is mathematically given as [27, 28]

$$\alpha = \alpha_0 \times \exp\left[-\left(\frac{T_0}{T}\right)^{\frac{1}{1+d}}\right], \tag{6}$$

where T_0 is the characteristic temperature and d is the dimensionality of the system. As Fig. 4 shows, $\ln(\alpha)$ follows a linear trend with $T^{-\frac{1}{4}}$, indicating that the spins probed by ESR are undergoing phonon-assisted hopping in 3D from 3.4 to 20 K. We find from our fit that T_0 is 17.9±5.5 K and that α_0 is 1.20. The asymptotic limit of the α parameter, α_0, approaches 1 as $T \to 0$. This trend is expected, since the asymmetry of the ESR signal is caused by thermally-activated hopping: as the phonon density decreases, so does the asymmetry of the Dysonian. The localization length, ξ, of the electronic wavefunction can be found from T_0 [28]

$$\xi = \left[\frac{18.1}{k_\mathrm{B} T_0 D(E_\mathrm{F})}\right]^{1/3}, \tag{7}$$

where $D(E_\mathrm{F})$ is the density of states around the Fermi energy, E_F. We can estimate $D(E_\mathrm{F})$ by treating the defect density of states as having an energy separation that can be roughly estimated by ΔE. Thus, $D(E_\mathrm{F}) \approx \frac{N(E_\mathrm{F})}{\Delta E} \sim 10^{19}$ states/cm^3-eV, where we are utilizing the spin density extracted from the Curie constant, $N(E_\mathrm{F}) = 1.14 \times 10^{16}$ spins/cm^3. From Eq. (7), we estimate ξ to be ∼100 nm, similar to previous measurements of defect-induced localization lengths in SWCNTs [44]. The spacing of defects, R_d, can be estimated by $\left(\frac{4\pi}{3}N\right)^{-1/3}$, or ∼28 nm. A $d = 3$ VRH behavior is expected in this wavefuncation-overlap regime ($R_\mathrm{d} < \xi$) [27]. In addition, in this regime, exchange effects may also be important, but defect concentration dependence is needed to investigate this avenue more fully.

It is important to note that given the difficulty in extracting α, the $T^{-1/4}$ trend that we are observing can be considered robust. We also performed traditional conductance measurements on a similarly prepared sample, and although the conductance clearly showed 3D VRH behavior, we believe that our ESR and four-point probe conductivity measurements are probing different species, since the hopping parameters do not agree and the high-T trends are different.

Finally, we note that the origin of the ESR signal is from SWCNTs, despite the fact that amorphous carbon, graphite, and other inhomogeneities are present in our sample. Unlike graphite, our observed ESR signal has a much lower g-factor. In addition, the T-dependence of the linewidth does not follow an Elliott-Yafet relaxation mechanism, as it does in graphite [35]. Similarly, we can discount the signal arising from amorphous carbon; in that system, the linewidth variation with T is not consistent with our observations [45].

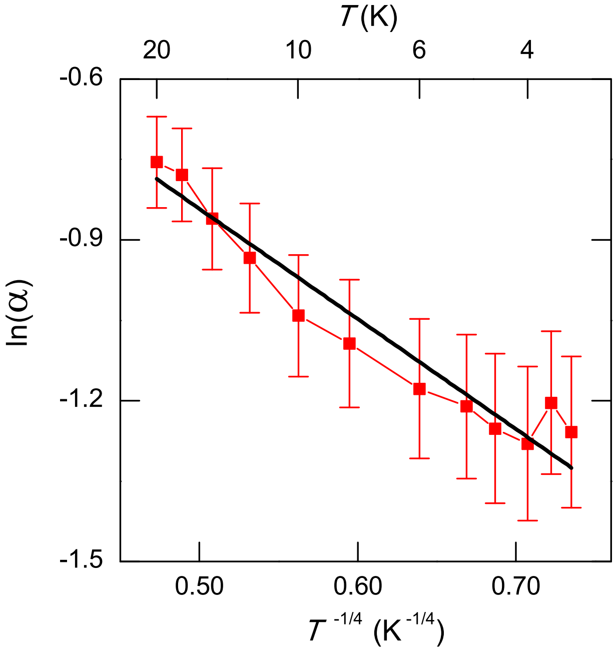

FIG. 4: (Color online) The natural log of the asymmetry Dysonian parameter, α, plotted against the fourth root of inverse temperature. The trend of $\ln(\alpha)$ follows a 3D VRH behavior, as given by the best fit line in black.

Although it is clear that the ESR signal arises from nanotubes, its microscopic origin is not certain. In a separate paper [22], we advocate that n-type defects are essential for the SWCNT ESR. We base this conclusion on the observation that ESR signal strongly depends on the presence of molecular oxygen (a p-type acceptor), an effect we find to be compatible with a compensation mechanism. This hypothesis is fully consistent with the data we present here. ESR-active defect states would explain the Curie-law dependence of χ_g, as well as the localized, phonon-assisted hopping of the spins and the motional narrowing of ΔH. In addition, our results are similar to those seen in doped semiconductors. The wide variety of SWCNT ESR results over the past two decades may be due to the different defect concentrations, which would change both the temperature dependence of the spin susceptibility and $\Delta H(T)$. Further work needs to be done to elucidate and clarify this hypothesis.

In summary, we have performed temperature-dependent ESR measurements on an ensemble of SWCNTs. We observe motional narrowing of the ESR linewidth in nanotubes for the first time. The spin susceptibility shows a $1/T$-type trend, confirming that the probed spins are localized species. An estimate of the spin density gives 0.58 spins per nanotube. We observe that the Dysonian asymmetry parameter, α, follows a $T^{-\frac{1}{4}}$ trend, which suggests 3D variable range hopping as the spin transport mechanism. From the extracted parameters, we estimate the localization length to be

∼100 nm with a density of states at the Fermi energy of $\sim 10^{19}$ states/eV-cm^3.

This work was supported by the DOE/BES through Grant No. DEFG02-06ER46308, the NSF through Grant Nos. OISE-0530220 and OISE-0968405, the Robert A. Welch Foundation through Grant No. C-1509, the Air Force Research Laboratories under contract number FA8650-05-D-5807, the W. M. Keck Program in Quantum Materials at Rice University, the Korean Ministry of Education, Science and Technology under the World Class University Program (R31-2008-10029), and the NIH National Heart, Lung, and Blood Institute through Grant No. HL095820. We thank Qimiao Si, Adilet Imambekov, Robert Hauge, and Vladimir Burka for useful discussions.

---

* kono@rice.edu; corresponding author.

[1] Q. Si, Phys. Rev. Lett. **78**, 1767 (1997); *ibid.* **81**, 3191 (1998).
[2] L. Balents and R. Egger, Phys. Rev. Lett. **85**, 3464 (2000); Phys. Rev. B **64**, 035310 (2001).
[3] A. A. Kiselev and K. W. Kim, Phys. Rev. B **61**, 13115 (2000).
[4] S. Rabello and Q. Si, Europhys. Lett. **60**, 882 (2002).
[5] A. De Martino *et al.*, Phys. Rev. Lett. **88**, 206402 (2002).
[6] B. Dóra *et al.*, Phys. Rev. Lett. **101**, 106408 (2008).
[7] D. P. DiVincenzo, Science **270**, 255 (1995).
[8] S. A. Wolf *et al.*, Science **294**, 1488 (2001).
[9] T. Giamarchi, *Quantum Physics in One Dimension* (Oxford University Press, Oxford, 2004).
[10] T. Ando, J. Phys. Soc. of Japan **69**, 1757 (2000).
[11] M. Kosaka *et al.*, Chem. Phys. Lett. **233**, 47 (1995).
[12] P. Petit *et al.*, Phys. Rev. B **56**, 9275 (1997).
[13] A. S. Claye *et al.*, Phys. Rev. B **62**, R4845 (2000).
[14] K. Shen, D. L. Tierney, and T. Peitraß, Phys. Rev. B **68**, 165418 (2003).
[15] J.-P. Salvetat *et al.*, Phys. Rev. B **72**, 075440 (2005).
[16] V. Likodimos *et al.*, Phys. Rev. B **76**, 075420 (2007).
[17] B. Corzilius *et al.*, Phys. Stat. Sol. (b) **245**, 2251 (2008).
[18] N. Bloembergen, E. M. Purcell, and R. V. Pound, Phys. Rev. **73**, 679 (1948).
[19] R. Kubo and K. Tomita, J. Phys. Soc. Japan **9**, 888 (1954).
[20] F. J. Dyson, Phys. Rev. **98**, 349 (1955).
[21] P. Nikolaev *et al.*, J. Phys. Chem. C **111**, 17678 (2007).
[22] W. D. Rice *et al.*, arXiv1110.5220v1 (2011).
[23] V. Sitaram *et al.*, Phys. Rev. B **72**, 035209 (2005).
[24] P. W. Anderson and P. R. Weiss, Rev. Mod. Phys. **25**, 269 (1953).
[25] P. W. Anderson, J. Phys. Soc. Japan **9**, 316 (1954).
[26] A. Miller and E. Abrahams, Phys. Rev. **120**, 745 (1960).
[27] N. F. Mott, Phil. Mag. **19**, 835 (1969).
[28] H. Kamimura and H. Aoki, *The Physics of Interacting Electrons in Disordered Systems* (Clarendon Press, New York, NY USA, 1989), 1st ed.
[29] D. K. Wilson, Phys. Rev. **134**, A265 (1964).
[30] K. Morigaki and T. Mitsuma, J. Phys. Soc. Jpn. **20**, 62 (1965).
[31] C. Kittel, *Introduction to Solid State Physics* (John Wiley and Sons, Inc., New York, NY USA, 1996), 7th ed.
[32] G. Feher, Phys. Rev. **114**, 1219 (1959).
[33] S. Maekawa and N. Kinoshita, J. Phys. Soc. Japan **20**, 1447 (1965).
[34] Y. Ochiai and E. Matsuura, Phys. Stat. Sol. (a) **38** (1976).
[35] G. Wagoner, Phys. Rev. **118**, 647 (1960).
[36] M. Nechtschein *et al.*, Phys. Rev. B **27**, 61 (1983).
[37] K. Matsubara, T. Tsuzuku, and K. Sugihara, Phys. Rev. B **44**, 11845 (1991).
[38] K. Mizoguchi *et al.*, Phys. Rev. B **51**, 8864 (1995).
[39] A. J. Epstein *et al.*, Syn. Metals **21**, 63 (1987).
[40] Q. Li, L. Cruz, and P. Phillips, Phys. Rev. B **47**, 1840 (1993).
[41] H. Ue and S. Maekawa, Phys. Rev. B **3**, 4232 (1971).
[42] M. N. Alexander and D. F. Holcomb, Rev. Mod. Phys. **40**, 815 (1968).
[43] J. D. Quirt and J. R. Marko, Phys. Rev. B **5**, 1716 (1972).
[44] C. Gómez-Navarro *et al.*, Nat. Mat. **4**, 534 (2005).
[45] F. Demichelis *et al.*, Diam Relat. Mater. **3**, 844 (1994).